

Measuring effective electroweak couplings in single top production at the LHC

D. Espriu* and J. Manzano†

Departament d'Estructura i Constituents
de la Matèria and IFAE,
Universitat de Barcelona,
Diagonal, 647, E-08028 Barcelona

Abstract

We study the mechanism of single top production at the LHC in the framework of an effective electroweak Lagrangian, analyzing the sensitivity of different observables to the magnitude of the effective couplings that parametrize new physics beyond the Standard Model. The observables relevant to the distinction between left and right effective couplings involve in practice the measurement of the spin of the top and this can be achieved only indirectly by measuring the angular distribution of its decay products. We show that the presence of effective right-handed couplings implies that the top is not in a pure spin state. A unique spin basis is singled out which allows one to connect top decay products angular distribution with the polarized top differential cross section. We present a complete analytical expression of the differential polarized cross section of the relevant perturbative subprocess including general effective couplings. The mass of the bottom quark, which actually turns out to be more relevant than naively expected, is retained. Finally we analyze different aspects the total cross section relevant to the measurement of new physics through the effective couplings. The above analysis also applies to anti-top production in a straightforward way.

UB-ECM-PF 01/03

June 2001

*espriu@ecm.ub.es

†manzano@ecm.ub.es

1 Introduction

The standard model of electroweak and strong interactions has been, to this day, tested to a remarkable degree of accuracy, particularly in what concerns the neutral current sector. However it is clear that suffers from several theoretical drawbacks (naturalness, triviality,...) making it conceivable that it should be considered as an effective theory valid only at low energies ($\lesssim 1$ TeV). With the current limit on the Higgs mass already placed at 113,5 GeV [1] and no clear evidence for the existence of an elementary scalar (despite much controversy regarding the results of the last days of LEP) it makes sense to envisage an alternative to the minimal Standard Model described by an effective theory without any physical light scalar fields. This in spite of the seemingly good agreement between experiment and radiative corrections computed in the framework of the minimal Standard Model (see [2] however). This effective theory should contain an infinite set of effective operators, of increasing dimensionality, compatible with the electroweak and strong symmetries $SU(3)_c \times SU(2)_L \times U(1)_Y$ and their coefficients would parametrize physics beyond the Standard Model. In this framework [3] one can describe the low energy physics of theories exhibiting the pattern of symmetry breaking $SU(2)_L \times U(1)_Y \rightarrow U(1)_{em}$ with full generality, in the understanding, that this approach is useful as long as those particles not explicitly included in the effective Lagrangian are much heavier than the scale of energies at which the effective Lagrangian is to be used.

In this work we plan to investigate the new features that physics beyond the standard model may introduce in the production of the top (or anti-top) quarks through W -gluon fusion at the LHC. When describing the appropriate effective vertex in the effective Lagrangian language, we will keep only the leading non-universal (i.e. not appearing in the standard model) effective operators in the low energy expansion. They correspond to the operators of dimension four, which were first classified by Appelquist et al. [4]. These operators realize the $SU(2)_L \times U(1)_Y$ symmetry non-linearly and are thus characteristic of strongly coupled theories and, strictly speaking, are absent in the minimal Standard Model and modifications thereof containing only light fields, such as supersymmetric extensions, where all degrees of freedom are weakly interacting and need to be included explicitly. When particularizing to interactions involving the W, Z bosons, the operators present in the effective electroweak Lagrangian induce effective vertices coupling the gauge boson to the matter fields (see e.g. [5])

$$- \frac{e}{4c_W s_W} \bar{f} \gamma^\mu (\kappa_L^{NC} L + \kappa_R^{NC} R) Z_\mu f - \frac{e}{s_W} \bar{f} \gamma^\mu (\kappa_L^{CC} L + \kappa_R^{CC} R) \frac{\tau^-}{2} W_\mu^+ f + h.c. \quad (1)$$

Other possible effects are not physically observable, as we shall see in a moment. In practical terms, LHC will set bounds on these effective W vertices, and therefore our results are also relevant in a broader phenomenological context as a way to bound κ_L and κ_R , without any

need to appeal to an underlying effective Lagrangian describing a specific model of symmetry breaking. Of course one then loses the power of an effective Lagrangian, namely a well defined set of counting rules and the ability to relate different processes.

Another point to note is that, even in the minimal Standard Model, radiative corrections induce modifications in the vertices. Assuming a smooth dependence in the external momenta these form factors can be expanded in powers of momenta. At the lowest order in the derivative expansion, the effect of radiative corrections can be encoded in the effective vertices κ_L and κ_R . Thus these effective vertices take well defined, calculable values in the minimal Standard Model, and any deviation from these values (which, incidentally, have not been yet fully determined in the Standard Model yet) would indicate the presence of new physics in the matter sector. The extent to what LHC can set direct bounds on the effective vertices, in particular on those involving the third generation, is highly relevant to constraint physics beyond the Standard Model in a direct way. This paper is devoted to such an analysis in charged processes involving a top quark at the LHC.

At the LHC energy (14 TeV) the dominant mechanism of top production, with a cross section of 800 pb[6], is gluon-gluon fusion. This mechanism has nothing to do with the electroweak sector and thus is not the most adequate for our purposes (although is the one producing most of the tops and thus its consideration becomes necessary in order to study the top couplings through their decay, which will not be our main interest here, and also as a background to the process we shall be interested in).

Electroweak physics enters the game in single top production. (For a recent review see e.g. [7].) At LHC energies the (by far) dominant electroweak subprocess contributing to single top production is given by a gluon (g) coming from one proton and a light quark or anti-quark coming from the other (this process is also called t -channel production [8, 9]). This process is depicted in Figs. 1 and 2, where light u -type quarks or \bar{d} -type antiquarks are extracted from the proton, respectively. These quarks then radiate a W whose effective couplings is the object of our interest. The cross total section for this process at the LHC is estimated to be 250 pb[9], to be compared to 50 pb for the associated production with a W^+ boson and a b -quark extracted from the sea of the proton, and 10 pb corresponding to quark-quark fusion (s -channel production). For comparison, at the Tevatron (2 GeV) the cross section for W -gluon fusion is 2.5 pb, so the production of tops through this particular subprocess is copious at the LHC. Monte Carlo simulations including the analysis of the top decay products indicate that this process can be analyzed in detail at the LHC and traditionally has been regarded as the most important one for our purposes.

In a proton-proton collision a bottom-anti-top pair is also produced, through the subprocesses given in Figs. 3 and 4. At any rate qualitative results are very similar to those

corresponding to top production, from where the cross sections can be easily derived doing the appropriate changes.

In the context of effective theories, the contribution from operators of dimension five to top production via longitudinal vector boson fusion was estimated some time ago in [11], although the study was by no means complete. It should be mentioned that t, \bar{t} pair production through this mechanism is very much masked by the dominant mechanism of gluon-gluon fusion, while single top production, through WZ fusion, is expected to be much suppressed compared to the mechanism presented in this paper, the reason being that both vertices are electroweak in the process discussed in [11], and that operators of dimension five are expected to be suppressed, at least at moderate energies, by some large mass scale. The contribution from dimension four operators as such has not, to our knowledge, been considered before, although the potential for single top production for measuring the CKM matrix element K_{tb} , has to some extent been analyzed in the past (see e.g. [9, 10]).

2 Effective couplings and observables

Including family mixing and, possibly, CP violation, the complete set of dimension four effective operators which may contribute to the top effective couplings and are relevant for the present discussion is [4, 12, 13]

$$\begin{aligned}\mathcal{L}_L^1 &= i\bar{f}M_L^1\gamma^\mu U(D_\mu U)^\dagger Lf + h.c., \\ \mathcal{L}_L^2 &= i\bar{f}M_L^2\gamma^\mu(D_\mu U)\tau^3 U^\dagger Lf + h.c., \\ \mathcal{L}_L^3 &= i\bar{f}M_L^3\gamma^\mu U\tau^3 U^\dagger(D_\mu U)\tau^3 U^\dagger Lf + h.c., \\ \mathcal{L}_L^4 &= i\bar{f}M_L^4\gamma^\mu U\tau^3 U^\dagger D_\mu^L Lf + h.c.,\end{aligned}\tag{2}$$

and

$$\begin{aligned}\mathcal{L}_R^1 &= i\bar{f}M_R^1\gamma^\mu U^\dagger(D_\mu U)Rf + h.c., \\ \mathcal{L}_R^2 &= i\bar{f}M_R^2\gamma^\mu\tau^3 U^\dagger(D_\mu U)Rf + h.c., \\ \mathcal{L}_R^3 &= i\bar{f}M_R^3\gamma^\mu\tau^3 U^\dagger(D_\mu U)\tau^3 Rf + h.c.,\end{aligned}\tag{3}$$

where $L = \frac{1-\gamma^5}{2}$, $R = \frac{1+\gamma^5}{2}$ are the left and right projectors, the matrices M have family indices only, and the above set is written in the non-physical ‘weak’ basis (that is, with matter fields transforming as irreducible representations of the gauge group) [13]. The unitary matrix U contains the three Goldstone bosons associated to the breakdown of the global symmetry $SU(2)_L \times SU(2)_R$ down to $SU(2)_V$. The derivatives appearing in the effective operators are given by

$$D_\mu U = \partial_\mu U + ig\frac{\tau}{2} \cdot W_\mu U - ig'U\frac{\tau^3}{2}B_\mu,$$

$$\begin{aligned}
D_\mu^L f &= \left(\partial_\mu + ig \frac{\tau}{2} \cdot W_\mu + ig' \left(Q - \frac{\tau^3}{2} \right) B_\mu + ig_s \frac{\lambda}{2} \cdot G_\mu \right) f, \\
D_\mu^R f &= \left(\partial_\mu + ig' Q B_\mu + ig_s \frac{\lambda}{2} \cdot G_\mu \right) f,
\end{aligned} \tag{4}$$

where f is a weak doublet of matter fields with family indices also. In addition, one has the following ‘universal’ terms

$$\begin{aligned}
\mathcal{L}_{SM} &= i \bar{f} \gamma^\mu \left[M^L D_\mu^L L + \left(\tau^u M_u^R + \tau^d M_d^R \right) D_\mu^R R \right] f \\
&\quad - \bar{f} \left(U \left(\tau^u \tilde{y}_u^f + \tau^d \tilde{y}_d^f \right) R + \left(\tau^u \tilde{y}_u^{f\dagger} + \tau^d \tilde{y}_d^{f\dagger} \right) U^\dagger L \right) f,
\end{aligned} \tag{5}$$

which are present in the Standard Model. In Eq.(5) we allow for general couplings M_L , $M_R^{(u,d)}$; in the Standard Model these couplings can be renormalized away via a change of basis, but in more general theories they leave traces in other operators not present in the Standard Model[13].

In [13] it was also shown that when we diagonalize the mass matrix present in Eq. (5) via a redefinition of the matter fields ($f \rightarrow f$) we change also the structure of operators (2,3). Taking that into account, the contribution to the different gauge boson-fermion-fermion vertices is as follows

$$\begin{aligned}
\mathcal{L}_{bff} &= -g_s \bar{f} \gamma^\mu (a_L L + a_R R) \frac{\lambda}{2} \cdot \mathbf{G}_\mu f, \\
&\quad - e \bar{f} \gamma^\mu (b_L L + b_R R) A_\mu f, \\
&\quad - \frac{e}{2c_W s_W} \bar{f} \gamma^\mu \left[\left(c_L^u \tau^u + c_L^d \tau^d \right) L + \left(c_R^u \tau^u + c_R^d \tau^d \right) R \right] Z_\mu f \\
&\quad - \frac{e}{s_W} \bar{f} \gamma^\mu \left[(d_L L + d_R R) \frac{\tau^-}{2} W_\mu^+ + \left(d_L^\dagger L + d_R^\dagger R \right) \frac{\tau^+}{2} W_\mu^- \right] f,
\end{aligned} \tag{6}$$

where τ^u and τ^d are the up and down projectors and f represents the matter fields in the physical, diagonal basis. It can be shown that once the all the renormalization (vertex, CKM elements, wave-function) counterterms are taken into account [13] we obtain $a_{L,R} = 1$, $b_{L,R} = Q$; i.e. we have no contribution from the effective operators to the vertices of the gluon and photon. For the Z couplings we get instead

$$\begin{aligned}
c_L^u &= 1 - 2Qs_W^2 - N^1 - N^{1\dagger} + N^{2\dagger} + N^2 + N^3 + N^{3\dagger}, \\
c_L^d &= -1 - 2Qs_W^2 + K^\dagger \left(N^1 + N^{1\dagger} + N^{2\dagger} + N^2 - N^3 - N^{3\dagger} \right) K, \\
c_R^u &= -2s_W^2 Q + \tilde{M}^1 + \tilde{M}^{1\dagger} + \tilde{M}^2 + \tilde{M}^{2\dagger} + \tilde{M}^3 + \tilde{M}^{3\dagger}, \\
c_R^d &= -2s_W^2 Q + \tilde{M}^1 + \tilde{M}^{1\dagger} - \tilde{M}^2 - \tilde{M}^{2\dagger} - \tilde{M}^3 - \tilde{M}^{3\dagger},
\end{aligned} \tag{7}$$

where K is the CKM matrix, and the matrices N ’s and \tilde{M} ’s are redefined matrices according to the results of [13] (the exact relation of these matrices to the M ’s of Eqs. (2,3) has no

relevance for the present discussion). Finally for the charged couplings we have

$$\begin{aligned} d_L &= K + \left(-N^1 - N^{1\dagger} + N^2 - N^{2\dagger} - N^3 - N^{3\dagger} + N^4 - N^{4\dagger} \right) K, \\ d_R &= \tilde{M}^1 + \tilde{M}^{1\dagger} + \tilde{M}^2 - \tilde{M}^{2\dagger} - \tilde{M}^3 - \tilde{M}^{3\dagger}. \end{aligned} \quad (8)$$

Since the set of operators (2-3) is the most general one allowed by general requirements of gauge invariance, locality and hermiticity; it is clear that radiative corrections, when expanded in powers of p^2 , can be incorporated into them. In fact, such an approach has proven to be very fruitful in the past. Once everything is included we are allowed to identify the couplings $d_{L,R}$ with κ_{LR}^{CC} . In this paper we shall be concerned with the bounds that the LHC experiments will be able to set on the couplings κ_{LR}^{CC} , more specifically on the entries tj of these matrices (those involving the top). In the rest of the article we do not consider mixing and we consider non-tree level and new physics contributions only on the tb effective couplings, therefore in the numerical simulations we have taken

$$\begin{aligned} d_L &= \text{diag} (K_{ud}, K_{cs}, g_L), \\ d_R &= \text{diag} (0, 0, g_R). \end{aligned}$$

When we speak along the paper of the results for the Standard Model at tree level we mean $g_L = 1$, and $g_R = 0$. However, even though numerical results are presented considering only the tb entry (g_L and g_R), since flavour indices and masses are kept all along in the analytical expressions (see Appendix), the appropriate changes to include other entries are immediate.

The effective couplings of the neutral sector (7) can be determined from the $Z \rightarrow f \bar{f}$ vertex¹ [12], but at present not much is known from the tb effective coupling. This is perhaps best evidenced by the fact that the current experimental results for the (left-handed) K_{tb} matrix element give [14]

$$\frac{|K_{tb}|^2}{|K_{td}|^2 + |K_{ts}|^2 + |K_{tb}|^2} = 0.99 \pm 0.29. \quad (9)$$

In the Standard Model this matrix element is expected to be close to 1. It should be emphasized that these are the ‘measured’ or ‘effective’ values of the CKM matrix elements, and that they do not necessarily correspond, even in the Standard Model, to the entries of a unitary matrix on account of the presence of radiative corrections. These deviations with respect to unitarity are expected to be small —at the few per cent level at most— unless new physics is present. At the Tevatron the left-handed couplings are expected to be eventually measured with a 5% accuracy [15]. The present work is a contribution to such an analysis in the case of the LHC experiments.

¹A 3 σ discrepancy with respect to the Standard Model results, mostly due to the right-handed coupling, remains in the Z couplings of the b quark to this date.

As far as experimental bounds for the right handed effective couplings is concerned, the more stringent ones come at present from the measurements on the $b \rightarrow s\gamma$ decay at CLEO [16]. Due to a m_t/m_b enhancement of the chirality flipping contribution, a particular combination of mixing angles and κ_R^{CC} can be found. The authors of [17] reach the conclusion that $|\text{Re}(\kappa_R^{CC})| \leq 0.4 \times 10^{-2}$. However, considering κ_R^{CC} as a matrix in generation space, this bound only constraints the tb element. Other effective couplings involving the top remain virtually unrestricted from the data. The previous bound on the right-handed coupling is a very stringent one. It is pretty obvious that the LHC will not be able to compete with such a bound. Yet, the measurement will be a direct one, not through loop corrections. Equally important is that it will yield information on the td and ts elements too, by just replacing the \bar{b} quark in Figs. 1,2 by a \bar{d} or a \bar{s} respectively.

Now we shall proceed to analyze the bounds that single top production at the LHC can set on the effective couplings. This combined with the data from Z physics will allow an estimation of the six effective couplings (7-8) in the matter sector of the effective electroweak Lagrangian. We will, in the present work limit ourselves to the consideration of the cross-sections for production of polarized top quarks. We shall not consider at this stage the potential of measuring top decays angular distributions in order to establish relevant bounds on the effective electroweak couplings. This issue merits a more detailed analysis, including the possibility of detecting CP violation [18].

3 The cross section

In order to calculate the cross section σ of the process $pp \rightarrow t\bar{b}$ we have used the CTEQ4 set of structure functions [19] to determine the probability of extracting a parton with a given fraction of momenta from the proton. Hence we write schematically

$$\sigma = \sum_q \int_0^1 \int_0^1 f_g(y) f_q(x) \hat{\sigma}(xP_1, yP_2) dx dy, \quad (10)$$

where f_q denote the parton distribution function (PDF) corresponding to the partonic quarks and antiquarks and f_g indicate the PDF corresponding to the gluon. In Eq.(10) we have set the light quark and gluon momenta to xP_1 and yP_1 , respectively. (P_1 and P_2 are the four-momenta of the two colliding protons.) The approximation thus involves neglecting the transverse momenta of the incoming partons; the transverse fluctuations are integrated over by doing the appropriate integrals over k_T . We have then proceeded as follows. We have multiplied the parton distribution function of a gluon of a given momenta from the first proton by the sum of parton distribution functions for obtaining a u type quark from the second proton. This result is then multiplied by the cross sections of the subprocesses of

Fig.1. We perform also the analogous process with the \bar{d} type anti-quarks of Fig.2. At the end, these two partial results are add up to obtain the total $pp \rightarrow t\bar{b}$ cross section.

Typically the top quark decays weakly well before strong interactions become relevant, we can in principle measure its polarization state with virtually no contamination of strong interactions (see e.g. [20] for discussions this point and section 6). For this reason we have considered polarized cross sections and provide general formulas for the production of polarized tops or anti-tops. To this end one needs to introduce the spin projector

$$\left(\frac{1 + \gamma_5 \not{n}}{2} \right),$$

with

$$\begin{aligned} n^\mu &= \frac{1}{\sqrt{(p_1^0)^2 - (\vec{p}_1 \cdot \hat{n})^2}} (\vec{p}_1 \cdot \hat{n}, p_1^0 \hat{n}), \\ \hat{n}^2 &= 1, \quad n^2 = -1, \end{aligned}$$

as the polarization projector for a particle or anti-particle of momentum p_1 with spin in the \hat{n} direction. The calculation of the subprocesses cross sections have been performed for tops and anti-tops polarized in an arbitrary direction \hat{n} . Later we have analyzed numerically different spin frames defined as follows

- Lab helicity frame: the polarization vector is taken in the direction of the three momentum of the top or anti-top (right helicity) or in the opposite direction (left helicity).
- Lab spectator frame: the polarization vector is taken in the direction of the three momentum of the spectator quark jet or in the opposite direction. The spectator quark is the d -type quark in Fig.1 or the \bar{u} -type quark in Fig.2.
- Rest spectator frame: like in the Lab spectator frame we choose the spectator jet to define the polarization of the top or anti-top. Here, however, we define \hat{n} as \pm the direction of the three momentum of the spectator quark in the top or anti-top rest frame (given by a pure boost transformation Λ of the lab frame). Then we have $n_r = (0, \hat{n})$ in that frame and $n = \Lambda^{-1} n_r$ back to the lab frame.

The calculation of the subprocess polarized cross-section we present is completely analytical from beginning to end and the results are given in the Appendix. Both the kinematics and the polarization vector of the top (or anti-top) are completely general. Since the calculation is of a certain complexity a number of checks have been done to ensure that no mistakes have been made. The integrated cross section agrees well with the results in [9] when the same cuts, scale, etc. are used. The mass of the top is obviously kept, but so is the bottom mass.

The latter in fact turns out to be more relevant than expected as we shall see in a moment. As we have already discussed, the production of flavours other than \bar{b} in association with the top can be easily derived from our results.

In single top production a distinction is often made between $2 \rightarrow 2$ and $2 \rightarrow 3$ processes. The latter corresponds, in fact, to the processes we have been discussing, the ones represented in Fig.1, in which a gluon from the sea splits into a $b \bar{b}$ pair. In the $2 \rightarrow 2$ process the b quark is assumed to be extracted from the sea of the proton, and both b and \bar{b} are collinear. Of course since the proton has no net b content, a \bar{b} quark must be present somewhere in the final state and the distinction between the two processes is purely kinematical. As is well known, when calculating the total cross section for single top production a logarithmic mass singularity [9] appears in the total cross section due to the collinear regime where the b quark (and the \bar{b}) quark have $k_T \rightarrow 0$. This kinematic singularity is actually regulated by the mass of the bottom; it appears to all orders in perturbation theory and a proper treatment of this singularity requires the use of the Altarelli-Parisi equations and its resummation into a b parton distribution function. It is thus indistinguishable of the so-called $2 \rightarrow 2$ process. Clearly an appropriate cut in k_T should allow us to retain the perturbative regime of the $2 \rightarrow 3$ process, while suppressing the $2 \rightarrow 2$ one.

Two approaches can be used at this point. One —advocated by Willenbrock and coworkers [9] is to focus on the low p_T regime, to minimize the contribution of the t, \bar{t} background. One actually is interested in processes where one does not see the \bar{b} (resp. b) quark which is produced in association with the t quark (resp. \bar{t}), and therefore sets an upper cut on the p_T of the \bar{b} . For this one has to take into account the $2 \rightarrow 2$ process and, in particular, one must pay attention not to double count the low p_T region (for the \bar{b} (or b) quark) of the $2 \rightarrow 3$ process, which is already included via a b PDF. The reason given in [9] is to separate this single top production process from the dominant $gg \rightarrow \bar{t}t$, which eventually also produces a b and a \bar{b} . We view this strategy as somewhat risky since, first of all, the separation between the $2 \rightarrow 3$ and $2 \rightarrow 2$ is not a clear cut one and, on top of that, it is a region where the cross section is rapidly varying so the results do depend on the way the separation is done. Furthermore it relies on assuming that we have a good knowledge of the b PDF at that scale; one will be forced to assume that it behaves largely like the s PDF at the end of the day. On top of that, that strategy does not completely avoid the background originated in $\bar{t}t$ production. That is, when in the decaying $\bar{t} \rightarrow W^- \bar{b} \rightarrow \bar{u} d \bar{b}$ the \bar{b} is missed along with the \bar{u} -type anti-quark in which case the d -type quark is taken as the spectator or when the \bar{b} is missed along with the d -type quark in which case the \bar{u} -type anti-quark is taken as the spectator.

On the other hand, measuring the \bar{b} (or b for anti-top production) momenta will allow

a better kinematic reconstruction of the individual processes. This should allow for a separation from the dominant mechanism of top production through gluon fusion. Setting a sufficiently high cut for the jet energy and a good jet separation should be sufficient to avoid contamination from t, \bar{t} when one hadronic jet is missed. Finally, the spin structure of the top is completely different in both cases due to the chiral couplings in electroweak production. Therefore, according to this philosophy —stay perturbative—, we have implemented a lower cut of 30 GeV in the transversal momentum of the \bar{b} (resp. b) in top (resp. anti-top) production.

4 A first look at the results

We shall now present the results of our analysis. To calculate the total event production corresponding to different observables we have used the integrating montecarlo program VEGAS [22]. We present results after one year (defined as 10^7 seg.) run at full luminosity in one detector (100 fb^{-1} at LHC).

The total contribution to the electroweak vertices g_L, g_R has two sources: the effective operators parametrizing new physics, and the contribution from the universal radiative corrections. In the standard model, neglecting mixing, for example, we have a tree level contribution to the $\bar{t}W_\mu^+b$ vertex given by $-\frac{i}{\sqrt{2}}\gamma_\mu g K_{tb}L$. Radiative corrections (universal and M_H dependent) modify g_L and generate a non zero g_R . These radiative corrections depend weakly on the energy of the process and thus in a first approximation we can take them as constant. Our purpose is to estimate the dependence of different LHC observables on these total effective couplings and how the experimental results can be used to set bounds on them. Assuming that the radiative corrections are known, this implies in turn a bound on the coefficients of the effective electroweak Lagrangian.

Let us start by discussing the experimental cuts. Due to geometrical detector constraints we cut off very low angles for the outgoing particles. The top, anti-bottom, and spectator quark have to come out with an angle of less than 10 degrees and more than 170 degrees. These angular cuts correspond to a cut in pseudorapidity $|\eta| < 2.44$. In order to be able to detect the three jets corresponding to the outgoing particles we implements isolation cuts of 20 degrees between each other.

As already discussed we use a lower cut of 30 GeV in the \bar{b} jet. This reduces the cross section to less than one third of its total value, since typically the \bar{b} quark comes out in the same direction as the incoming muon and a large fraction of them do not pass the cut. Similarly, $p_T > 20$ GeV cuts are set for the top and spectator quark jets. These cuts guarantee the validity of perturbation theory and will serve to separate from the overwhelming

background of low p_T physics. These values come as a compromise to preserve a good signal, while suppressing unwanted contributions. They are similar, but not identical to the ones used in [9] and [10]. To summarize

$$\begin{aligned}
\text{detector geometry cuts} & : 10^\circ \leq \theta_i \leq 170^\circ, \quad i = t, \bar{b}, q_s, \\
\text{isolation cuts} & : 20^\circ \leq \theta_{ij}, \quad i, j = t, \bar{b}, q_s, \\
\text{theoretical cuts} & : 20 \text{ GeV} \leq p_1^T, \quad 20 \text{ GeV} \leq q_2^T, \quad 30 \text{ GeV} \leq p_2^T, \quad (11)
\end{aligned}$$

where $\theta_t, \theta_{\bar{b}}, \theta_{q_s}$ are the polar angles with respect to the beam line of the top, anti-bottom and spectator quark respectively; $\theta_{t\bar{b}}, \theta_{tq_s}, \theta_{\bar{b}q_s}$ are the angles between top and anti-bottom, top and spectator, and anti-bottom and spectator, respectively. The momenta conventions are given in Figs.1-4.

Numerically, the dominant contribution to the process comes from the diagram where a b quark is exchanged in the t channel, but a large amount of cancellation takes place with the crossed interference term with the diagram with a top quark in the t channel. The smallest contribution (but obviously non-negligible) corresponds to this last diagram. It is then easy to see, given the relative smallness of the b mass, why the process is so much forward.

Undoubtedly the largest theoretical uncertainty in the whole calculation is the choice of a scale for α_s and the PDF's. We perform a leading order calculation in QCD and the scale dependence is large. We have made two different choices. We present some results with the scale p_T^{cut} used in α_s and the gluon PDF, while the virtuality of the W boson is used as scale for the PDF of the light quarks in the proton. When we use these scales and compute, for instance, the total cross section above a cut of $p_T = 20$ GeV in the \bar{b} momentum, we get an excellent agreement with the calculations in [9]. Most of our results are however presented with a common scale $\mu^2 = \hat{s}$, \hat{s} being the center-of-mass energy squared of the qg subprocess. The total cross section above the cut is then roughly speaking two thirds of the previous one, but no substantial change in the distributions takes place. It remains to be seen which one is the correct choice.

From our Monte Carlo simulation for single top production at the LHC after 1 year of full luminosity and with the cuts given above we obtain the total number of events. This number depends on the value of the effective couplings and on the top polarization vector n given in the frames defined in section 3. If we call $N(g_L, g_R, \hat{n}, (frame))$ to this quantity, we obtain the following results

$$\begin{aligned}
N\left(g_L, g_R, \hat{n} = \pm \frac{\vec{p}_1}{|\vec{p}_1|}, (lab)\right) & = g_L^2 \times (3.73 \mp 1.31) \times 10^5 + g_R^2 \times (3.54 \pm .97) \times 10^5 \\
& \quad + g_L g_R \times (-.237 \mp .0283) \times 10^5, \\
N\left(g_L, g_R, \hat{n} = \pm \frac{\vec{q}_2}{|\vec{q}_2|}, (lab)\right) & = g_L^2 \times (3.73 \pm 2.22) \times 10^5 + g_R^2 \times (3.54 \mp 2.12) \times 10^5
\end{aligned}$$

$$\begin{aligned}
& +g_L g_R \times (-.237 \mp 0.001) \times 10^5, \\
N\left(g_L, g_R, \hat{n} = \pm \frac{\vec{q}_2}{|\vec{q}_2|}, (rest)\right) &= g_L^2 \times (3.73 \pm 2.49) \times 10^5 + g_R^2 \times (3.54 \mp 2.15) \times 10^5 \\
& +g_L g_R \times (-.237 \mp .0180) \times 10^5,
\end{aligned} \tag{12}$$

where we have omitted the \sqrt{N} statistical errors and we have neglected possible CP phases (g_L and g_R real). One can observe from the simulations that the production of negative helicity (left) tops represents the 69% of the total single top production, this predominance of left tops in the tree level electroweak approximation is expected due to the suppression at high energies of right-handed tops because of the zero right coupling in the charged current sector. In fact the production of right-handed tops would be zero were it not for the chirality flip, due to the top mass, in the t -channel. Of course the name ‘left’ and ‘right’ are a bit misleading; we really mean negative and positive helicity states. Chirality states cannot be used, because the production is peaked in the 200 to 400 GeV region for the energy of the top and the mass cannot be neglected.

We have also calculated single anti-top production. In Fig.8 we show the histograms corresponding to the production of \bar{t} with the two possible helicities in the LAB frame. All the histograms correspond to the tree level electroweak approximation and clearly show that single anti-top production is approximately the 75% of single top production. The same pattern is observed in Fig. 9. This suppression is generated by the parton distribution functions corresponding to negatively charged quarks that are smaller than the ones corresponding to positively charged quarks. Because of that the conclusions for anti-top production are practically the same as the ones for top production taking into account this suppression and that, because of the transformations (27) (see Appendix), passing from top to anti-top is equivalent to changing the spin direction.

In Fig. 10 we plot the cross section distribution of the polar angles of the top and anti-bottom with respect to the beam line for unpolarized single top production at the LHC. In Fig. 11 we plot the distribution of the cosine of the angle between the top and the anti-bottom for unpolarized single top production at the LCH. Everything is calculated in the (tree-level) Standard Model in the LAB frame. In both figures the above cuts are implemented, in particular the isolation cut of 20 degrees in the angle between the top and the anti-bottom is clearly visible in Fig. 11. From inspection of these figures two facts emerge: a) the distribution is strongly peaked in the beam direction as expected. b) Even with the presence of the isolation cut, near the beam axis configurations with top and anti-bottom almost parallel are favoured with respect to back-to-back configurations. Therefore this is an indication that almost back-to-back configurations are distributed more uniformly in space than parallel configurations favoring the beam line direction.

Let us now depart from the tree-level Standard Model and consider non-zero values for δg_L and δg_R . . Our results can be summarized in Figs 14, 15, 16, 17

Taking into account the results of Eq. (12) we can establish the intervals where the effective couplings are indistinguishable from their tree level Standard Model values taking a 1 sigma deviation as a rough statistical criterion. Evidently we do not pretend to make here a serious experimental analysis since we are not taking into account the full set of experimental and theoretical uncertainties. Our aim is just to present an order of magnitude estimate of the sensitivity of the different spin basis to the value of the effective coupling around their tree level Standard Model value. The results are given in Table 1, where we indicate also the polarization vector chosen in each case. Of course those sensitivities (which, as said, are merely indicative) are calculated with the assumption that one could perfectly measure the top polarization in any of the above basis. As it is well known the top polarization is only measurable in an indirect way through the angular distribution of its decay products. In section 6 we outline the procedure to use our results to obtain a final angular distribution for the polarized top decay products (we believe that some confusion exists on this point). Obtaining that angular distribution involves a convolution of the single top production cross section with the decay products angular distribution and because of that we expect the true sensitivity to become worse than the ones given in table 1. Obviously that true sensitivity must be independent of the spin basis one uses at an intermediate step (see section 6) so the whole discussion as to which is the best basis for the top polarization is academic. However it may still be useful to know that some basis are more sensitive to the effective couplings than others if one *assumes* (at least as a gedanken experiment) that the polarization of the top could be measured directly.

It is worth mentioning that the bottom mass, which appears in the cross section in crossed left-right terms, such as $m_b g_L g_R$, plays a crucial role in the actual determination of g_R . This is because from the $|\text{Re}(\kappa_R^{CC})| \leq 0.4 \times 10^{-2}$ bound [17] we expect $g_L g_R m_b > g_R^2 m_t$. Evidently for the ts or td couplings these terms are not expected to be so relevant.

5 The differential cross section for polarized tops

We define the matrix element of the subprocess of Figs.1, to 4 as M_+^d , $M_+^{\bar{u}}$, M_-^u , and $M_-^{\bar{d}}$, respectively. With these definitions the differential cross section for polarized tops σ can be written schematically as

$$\sigma = c \left(f_u |M_+^d|^2 + f_{\bar{d}} |M_+^{\bar{u}}|^2 \right),$$

where f_u and $f_{\bar{d}}$ denote the parton distribution functions corresponding to extracting a u -type quark and a \bar{d} -type quark respectively and c is a proportionality factor incorporating the

polarization frame	g_L	g_R
$\hat{n} = \pm \frac{\vec{p}_1}{ \vec{p}_1 }, lab$	[0.9993, 1.0007] (-)	[-0.015, 0.074] (+)
$\hat{n} = \pm \frac{\vec{q}_2}{ \vec{q}_2 }, lab$	[0.9994, 1.0006] (+)	[-0.013, 0.054] (-)
$\hat{n} = \pm \frac{\vec{q}_2}{ \vec{q}_2 }, rest$	[0.9994, 1.0006] (+)	[-0.012, 0.051] (-)

Table 1: Sensitivity of the polarized single top production to variations of the effective couplings. To calculate the intervals we have taken 1 sigma statistical deviations from tree level values as an order of magnitude criterion. Of course, given the uncertainties in the QCD scale, the overall normalization is dubious and the actual precision on g_L a lot less. The purpose of these figures is to illustrate the relative accuracy. Between parenthesis we indicate the spin direction taken to calculate each interval.

kinematical and measure factors. Now using our analytical results for the matrix elements given in the Appendix along with Eq. (27) and symmetries (28) we obtain

$$\begin{aligned}
\sigma &= cf_u \left[|g_L|^2 (a + a_n) + |g_R|^2 (b + b_n) + \frac{g_R^* g_L + g_R g_L^*}{2} (c + c_n) + i \frac{g_L^* g_R - g_R^* g_L}{2} d_n \right] \\
&\quad + cf_{\bar{d}} \left[|g_R|^2 (a - a_n) + |g_L|^2 (b - b_n) + \frac{g_R^* g_L + g_R g_L^*}{2} (c - c_n) - i \frac{g_L^* g_R - g_R^* g_L}{2} d_n \right] \\
&= \begin{pmatrix} g_L^* & g_R^* \end{pmatrix} A \begin{pmatrix} g_L \\ g_R \end{pmatrix},
\end{aligned}$$

where

$$A = c \begin{pmatrix} f_u (a + a_n) + f_{\bar{d}} (b - b_n) & \frac{1}{2} f_u (c + c_n + i d_n) + \frac{1}{2} f_{\bar{d}} (c - c_n - i d_n) \\ \frac{1}{2} f_u (c + c_n - i d_n) + \frac{1}{2} f_{\bar{d}} (c - c_n + i d_n) & f_u (b + b_n) + f_{\bar{d}} (a - a_n) \end{pmatrix}, \quad (13)$$

and where a, b, c, a_n, b_n, c_n and d_n are independent of the effective couplings g_R and g_L and the subscripts n indicate linear dependence on the top spin four-vector n . From Eq. (13) we observe that A is an Hermitian matrix and therefore it is diagonalizable with real eigenvalues. Moreover, from the positivity of σ we immediately arrive at the constraints

$$\det A \geq 0, \quad (14)$$

$$Tr A \geq 0, \quad (15)$$

that is

$$\begin{aligned}
&(f_u (a + a_n) + f_{\bar{d}} (b - b_n)) (f_u (b + b_n) + f_{\bar{d}} (a - a_n)) \\
&\geq \frac{1}{4} \left(c^2 (f_u + f_{\bar{d}})^2 + (c_n^2 + d_n^2) (f_u - f_{\bar{d}})^2 + 2cc_n (f_u^2 - f_{\bar{d}}^2) \right), \quad (16)
\end{aligned}$$

and

$$(f_u + f_{\bar{d}}) (a + b) + (f_u - f_{\bar{d}}) (a_n + b_n) \geq 0. \quad (17)$$

Note that it is not possible to saturate both constraints for the same configuration because this would imply a vanishing A which in turn would imply relations such as

$$\frac{a+b}{a_n+b_n} = \frac{f_{\bar{d}}-f_u}{f_{\bar{d}}+f_u} = \frac{a_n-b_n}{a-b},$$

which evidently do not hold. Moreover, since constraints (16) and (17) must be satisfied for any set of positive PDF's we immediately obtain the bounds

$$\begin{aligned} ab + a_nb_n - \frac{1}{4}(c^2 + c_n^2 + d_n^2) &\geq \left| a_nb + ab_n - \frac{1}{2}cc_n \right| \\ b^2 + a^2 - (b_n^2 + a_n^2) &\geq \frac{1}{2}(c^2 - (c_n^2 + d_n^2)). \end{aligned}$$

In order to have a 100% polarized top we need a spin four-vector n that saturates the constraint (14) (that is Eq.(16)) for each kinematical situation, that is we need $A(n)$ to have a zero eigenvalue which is equivalent to have a unitary matrix C satisfying

$$C^\dagger AC = \text{diag}(\lambda, 0),$$

for some positive eigenvalue λ . In general such n need not exist and, should it exist, is in any case independent of the effective couplings g_R and g_L . Moreover, provided this n exists there is only one solution (up to a global complex normalization factor α) for the pair (g_R, g_L) to the equation $\sigma = 0$, This solution is just

$$\begin{aligned} g_L &= \alpha C_{12}, \\ g_R &= \alpha C_{22}. \end{aligned} \tag{18}$$

Note that if one of the effective couplings vanishes we can take the other constant and arbitrary. However if both effective couplings are non-vanishing we would have a quotient g_R/g_L that would depend in general on the kinematics. This is not possible so we can conclude that for a non-vanishing g_R (g_L is evidently non-vanishing) it is not possible to have a pure spin state (or, else, only for fine tuned g_R a 100% polarization is possible).

To illustrate these considerations let us give an example: in the unphysical situation where $m_t \rightarrow 0$ it can be shown that there exists two solutions to the saturated constraint (14), namely

$$m_t n^\mu \rightarrow \pm \left(|\vec{p}_1|, p_1^0 \frac{\vec{p}_1}{|\vec{p}_1|} \right), \tag{19}$$

once we have found this result we plug it in the expression (18) and we find the solutions $(0, g_L)$ with g_L arbitrary for the $+$ sign and $(g_R, 0)$ with g_R arbitrary for the $-$ sign. That is, physically we have zero probability of producing a right handed top when we have only a left handed coupling and viceversa when we have only a right handed coupling. Note that in this

case it is clear that having both effective couplings non-vanishing would imply the absence of 100 % polarization in any spin basis. This can be understood in general remembering that the top particle forms in general an entangled state with the other particles of the process. Since we are tracing over the unknown spin degrees of freedom and over the flavors of the spectator quark we do not expect in general to end up with a top in a pure polarized state; although this is not impossible as it is shown in the last example.

In the physical situation where $m_t \neq 0$ (we use $m_t = 175.6$ GeV. and $m_b = 5$ GeV. in this paper) we have found that a spin basis with relatively high polarization is the one with the spin \hat{n} taken in the direction of the spectator quark in the top rest frame. This is in accordance to the results in [10]. In general the degree of polarization ($\frac{N_{+\hat{n}}}{N_{+\hat{n}}+N_{-\hat{n}}}$) depends not only on the spin frame but also on the particular cuts chosen. We have found that the lower cut for the transverse momentum of the bottom worsens the polarization degree but, in spite of that, from Eq.(12) we see that we have a 84% of polarization in the Standard Model ($g_L = 1, g_R = 0$) that is much bigger than the 69% obtained with the helicity frame. The above results follow the general trend of those presented by Mahlon and Parke [10], but in general, their degree of polarization is higher. We understand that this is due to the different cuts (in particular for the transversal momentum of the bottom) along with the different set of PDF's used in our simulations.

6 Measuring the top polarization from its decay products

A well know result in the tree level SM regarding the measure of the top polarization from its decay products is the formula that states the following: Given a top polarized in the \hat{n} direction in its rest frame, the lepton l^+ produced in the decay of the top via the process

$$t \rightarrow b (W^+ \rightarrow l^+ \nu_l), \quad (20)$$

presents an angular distribution [23]

$$\sigma_l = \alpha (1 + \cos \theta), \quad (21)$$

where α is a normalization factor and θ is the axial angle measured from the direction of \hat{n} . What can we do when the top is in a mixed state with no 100% polarization in any direction? The first naive answer would be: With any axis \hat{n} in the top rest frame the top will have a polarization p_+ (with $0 \leq p_+ \leq 1$) in that direction and a polarization $p_- = 1 - p_+$ in the opposite direction so the angular distribution for the lepton is

$$\sigma_l = \alpha (p_+ (1 + \cos \theta) + p_- (1 - \cos \theta))$$

$$\begin{aligned}
&= \alpha (1 + (p_+ - p_-) \cos \theta) \\
&= \alpha (1 + (2p_+ - 1) \cos \theta).
\end{aligned} \tag{22}$$

The problem with formula (22) is that the angular distribution for the lepton depends on the arbitrary chosen axis \hat{n} and this cannot be correct. The correct answer can be obtained by noting the following facts:

- Given an arbitrary chosen axis \hat{n} in the rest frame and the associated spin basis to it $\{|+\hat{n}\rangle, |-\hat{n}\rangle\}$ the top spin state is given by a 2×2 density matrix ρ

$$\rho = \rho_+ |+\hat{n}\rangle \langle +\hat{n}| + \rho_- |-\hat{n}\rangle \langle -\hat{n}| + b |+\hat{n}\rangle \langle -\hat{n}| + b^* |-\hat{n}\rangle \langle +\hat{n}|, \tag{23}$$

which is in general not diagonal ($b \neq 0$) and whose coefficients depend on the rest of kinematical variables determining the differential cross section.

- From the calculation of the polarized cross section *we only know* the diagonal elements $\rho_{\pm} = p_{\pm} = |M|_{\pm\hat{n}}^2 / (|M|_{+\hat{n}}^2 + |M|_{-\hat{n}}^2)$.
- Given ρ in any orthogonal basis determined (up to phases) by \hat{n} we can change to another basis that diagonalizes ρ . Since the top is a spin 1/2 particle, this basis will correspond to another direction \hat{n}_d .
- Once we have ρ diagonalized then Eq.(22) is trivially correct with $p_{\pm} = \rho_{\pm}$ and now θ is unambiguously measured from the direction of \hat{n}_d .

From the above facts the first question that comes to our minds is if there exists a way to determine \hat{n}_d without knowing the off-diagonal matrix elements of ρ . The answer is yes. It is an easy exercise of elementary quantum mechanics that given a 2×2 Hermitian matrix ρ the eigenvector with largest (lowest) eigenvalue correspond to the unitary vector that maximizes (minimizes) the bilinear form $\langle v | \rho | v \rangle$ constrained to $\{|v\rangle, \langle v | v \rangle = 1\}$. Since an arbitrary normalized $|v\rangle$ can be written (up to phases) as $|+\hat{n}\rangle$ and in that case $\rho_+ = p_+$ then the correct \hat{n}_d entering in Eq.(22) is the one that maximizes the differential cross section $|M|_{\hat{n}}^2$ for each kinematical configuration. At the end, the correct angular distribution for the leptons is given by the cross section for polarized tops *in this basis* (\hat{n}_d) convoluted with formula (21) (or improvements of it [21]).

The above analysis was carried out in the Standard Model ($g_R = 0$) but it is correct also for $g_R \neq 0$ using the complete formula for this case

$$\sigma_l = \alpha \left(1 + (p_+ - p_-) \cos \theta \left(1 - \frac{1}{4} |g_R|^2 h \left(\frac{M_W^2}{m_t^2} \right) \right) \right), \tag{24}$$

where $h \left(\frac{M_W^2}{m_t^2} \right) \simeq 0.566$ [23]. Formula (24) deserves some comments:

- First of all we remember that θ is the angle (in the top rest frame) between the \hat{n} that maximizes the difference $(p_+ - p_-)$ and the three momentum of the lepton.
- Taking into account the above comment and that $(p_+ - p_-)$ depends on g_L and g_R we see that also θ depends on g_L and g_R .
- From the computational point of view, formula (24) is not an explicit formula because involves a process of maximization for each kinematical configuration.
- In some works in the literature [10] formula (24) is presented for an arbitrary choice of the spin basis $\{|\pm\hat{n}\rangle\}$ in the top rest frame. This is incorrect because it does not take into account that, in general, the top spin density matrix is not diagonal.
- In a recent work [21] $O(\alpha_s)$ corrections are incorporated to the polarized top decay angular analysis. In this work the density matrix for the top spin is properly taken into account. To connect this work with ours we have to replace their polarization vector \vec{P} by $P\hat{n}_d$ where the magnitude of the top polarization P is just the spin asymmetry $\left(|M|_{+\hat{n}_d}^2 - |M|_{-\hat{n}_d}^2\right) / \left(|M|_{+\hat{n}_d}^2 + |M|_{-\hat{n}_d}^2\right)$ in our language. This taken into account, the density matrix the authors of [21] quote is in the basis $\{|+\hat{n}_{W^+}\rangle, |-\hat{n}_{W^+}\rangle\}$ where \hat{n}_{W^+} is a normal vector in the direction of the three momentum of the W^+ (in the top rest frame).

7 Conclusions

We have done a complete calculation of the subprocess cross sections for polarized tops or anti-tops including the right effective coupling and bottom mass corrections. We have used a $p_T > 30$ GeV. cut in the transverse momentum of the produced \bar{b} quark and, accordingly we have retained only the so called $2 \rightarrow 3$ process, for the reasons described in the text.

Our analysis here is completely general. No approximation is made. We use the most general set of couplings and, since our approach is completely analytical, we can describe the contribution from other intermediate quarks in the t channel, mixing, etc. Masses and mixing angles are retained. On the contrary, the analysis has to be considered only preliminary from an experimental point of view. No detailed study of the backgrounds has been made, except for the dominant $gg \rightarrow t\bar{t}$ process which has been considered to some extent (although again without quantitative evaluation).

Given the (presumed) smallness of the right handed couplings, the bottom mass plays a role which is more important than anticipated, as the mixed crossed $g_L g_R$ term, which actually is the most sensitive one to g_R is accompanied by a b quark mass. The statistical sensitivity to different values of this coupling is given in the text.

We present a variety of p_T and angular distributions both for the t and the \bar{b} quarks. Obviously, the top decays shortly after production, but we have not made detailed simulations of this part. In fact, the interest of this decay is obvious: one can measure the spin of the top through the angular distribution of the leptons produced in this decay. In the Standard Model, single top production gives a high degree of polarization (84 % in the optimal basis, with the present set of cuts). This is a high degree of polarization, but well below the 90+ claimed by Mahlon and Parke in [10]. We understand this being due to the presence of the 30 GeV. cut. In fact, if we remove this cut completely we get a 91 % polarization. Still below the result of [10] but in rough agreement (note that we do not include the $2 \rightarrow 2$ process). Inasmuch as they can be compared our results are in good agreement with those presented in [9] in what concerns the total cross-section. Two different choices for the strong scale μ^2 are presented.

In addition, it turns out that when $g_R \neq 0$ the top can never be 100% polarized. In other words, it is in a mixed state. In this case we show that a unique spin basis is singled out which allows one to connect top decay products angular distribution with the polarized top differential cross section.

Finally it should be mentioned that a previous study for this process in the present context was performed by the present authors[24] using the effective W approximation[25], in which the W is treated as a parton of the proton. While this is certainly not an exact treatment, it is expected to be sufficiently good for our purposes. In the course of this work we have found, however, a number of interesting differences. A detailed comparison with this practical and widely used approach will be given elsewhere.

8 Acknowledgments

We would like to thank A.Dobado, S.Forte, M.J.Herrero, J.R.Peláez and E.Ruíz-Morales for multiple discussions. We would also like to thank W.Hollik for encouragement and for allowing us to present preliminary results in the LHC CERN Workshop. J.M. acknowledges a fellowship from Generalitat de Catalunya, grant 1998FI-00614. Financial support from grants AEN98-0431, 1998SGR 00026 and EURODAPHNE is greatly appreciated.

A Subprocesses cross sections

In this appendix we present the analytical results obtained for the matrix elements corresponding to the processes of Figs.(1-4) as M_+^d , $M_+^{\bar{u}}$, M_-^u , and $M_-^{\bar{d}}$, respectively. Defining

$$g_+ = g_R,$$

$$g_- = g_L,$$

we have the square modulus

$$|M_-^u|^2 = g_s^2 \left(O_{11} A_{11} + O_{22} A_{22} + O_c \left(A_p^{(+)} + A_p^{(-)} + A_{m_t}^{(+)} + A_{m_t}^{(-)} + A_{m_b}^{(+)} + A_{m_b}^{(-)} \right) \right), \quad (25)$$

with

$$\begin{aligned} O_{11} &= \frac{1}{4(k_1 \cdot p_1)^2}, \\ O_{22} &= \frac{1}{4(k_1 \cdot p_2)^2}, \\ O_c &= \frac{1}{4(k_1 \cdot p_1)(k_1 \cdot p_2)}, \end{aligned} \quad (26)$$

and

$$\begin{aligned} A_{11} &= \frac{|g|^4 |K_{ud}|^2}{(k_2^2 - M_W^2)^2} \left\{ im_t^2 m_b \frac{g_L^* g_R - g_R^* g_L}{2} \varepsilon^{\mu\nu\alpha\beta} (k_1 - p_1)_\mu n_\nu q_{2\alpha} q_{1\beta} \right. \\ &\quad + m_t m_b \frac{g_R^* g_L + g_L^* g_R}{2} [m_t (q_2 \cdot (k_1 - p_1)) (q_1 \cdot n) \\ &\quad - m_t (q_1 \cdot (k_1 - p_1)) (q_2 \cdot n) - (q_1 \cdot q_2) (m_t^2 - (k_1 \cdot p_1))] \\ &\quad + 2|g_L|^2 (q_2 \cdot p_2) \left[\left(m_t^2 + \frac{p_1 + m_t n}{2} \cdot (k_1 - p_1) \right) (q_1 \cdot (k_1 - p_1)) \right. \\ &\quad \left. - \frac{1}{2} m_t^3 (n \cdot q_1) + \left(\frac{p_1 + m_t n}{2} \cdot q_1 \right) (k_1 \cdot p_1) \right] \\ &\quad + 2|g_R|^2 (q_1 \cdot p_2) \left[\left(m_t^2 + \frac{p_1 - m_t n}{2} \cdot (k_1 - p_1) \right) (q_2 \cdot (k_1 - p_1)) \right. \\ &\quad \left. + \frac{1}{2} m_t^3 (n \cdot q_2) + \left(\frac{p_1 - m_t n}{2} \cdot q_2 \right) (k_1 \cdot p_1) \right] \left. \right\}, \end{aligned}$$

and

$$\begin{aligned} A_{22} &= \frac{|g|^4 |K_{ud}|^2}{(k_2^2 - M_W^2)^2} \left\{ (k_1 \cdot p_2) \left[2|g_R|^2 (q_1 \cdot k_1) \left(q_2 \cdot \frac{p_1 - m_t n}{2} \right) \right. \right. \\ &\quad + 2|g_L|^2 (q_2 \cdot k_1) \left(q_1 \cdot \frac{p_1 + m_t n}{2} \right) \left. \right] \\ &\quad + m_b^2 \left[2|g_R|^2 (q_1 \cdot (k_1 - p_2)) \left(q_2 \cdot \frac{p_1 - m_t n}{2} \right) \right. \\ &\quad + 2|g_L|^2 (q_2 \cdot (k_1 - p_2)) \left(q_1 \cdot \frac{p_1 + m_t n}{2} \right) \left. \right] \\ &\quad + m_b \frac{g_L^* g_R + g_R^* g_L}{2} (m_b^2 - (k_1 \cdot p_2)) [-m_t (q_1 \cdot q_2) \\ &\quad - (q_1 \cdot n) (q_2 \cdot p_1) + (q_2 \cdot n) (q_1 \cdot p_1)] \\ &\quad \left. - im_b \frac{g_L^* g_R - g_R^* g_L}{2} (m_b^2 - (k_1 \cdot p_2)) \varepsilon^{\mu\nu\alpha\beta} n_\mu p_{1\nu} q_{2\alpha} q_{1\beta} \right\}, \end{aligned}$$

and

$$\begin{aligned}
A_p^{(\pm)} = & -\frac{|g|^4 |K_{ud}|^2}{(k_2^2 - M_W^2)^2} |g_{\pm}|^2 \left\{ (q_1 \cdot q_2) \left[((k_1 - p_1) \cdot (k_2 - p_1)) \left(\frac{p_1 \mp m_t n}{2} \cdot p_2 \right) \right. \right. \\
& + \left. \left((k_1 - p_1) \cdot \frac{p_1 \mp m_t n}{2} \right) ((k_2 - p_1) \cdot p_2) - ((k_1 - p_1) \cdot p_2) \left(\frac{p_1 \mp m_t n}{2} \cdot (k_2 - p_1) \right) \right] \\
& + ((k_2 - p_1) \cdot q_2) \left[(p_2 \cdot (k_1 - p_1)) \left(q_1 \cdot \frac{p_1 \mp m_t n}{2} \right) - (q_1 \cdot p_2) \left((k_1 - p_1) \cdot \frac{p_1 \mp m_t n}{2} \right) \right] \\
& - ((k_1 - p_1) \cdot q_2) \left[(p_2 \cdot (k_2 - p_1)) \left(q_1 \cdot \frac{p_1 \mp m_t n}{2} \right) - (q_1 \cdot p_2) \left((k_2 - p_1) \cdot \frac{p_1 \mp m_t n}{2} \right) \right] \\
& + ((k_2 - p_1) \cdot q_1) \left[(p_2 \cdot (k_1 - p_1)) \left(q_2 \cdot \frac{p_1 \mp m_t n}{2} \right) - (q_2 \cdot p_2) \left((k_1 - p_1) \cdot \frac{p_1 \mp m_t n}{2} \right) \right] \\
& - ((k_1 - p_1) \cdot q_1) \left[(p_2 \cdot (k_2 - p_1)) \left(q_2 \cdot \frac{p_1 \mp m_t n}{2} \right) - (q_2 \cdot p_2) \left((k_2 - p_1) \cdot \frac{p_1 \mp m_t n}{2} \right) \right] \\
& \pm ((k_1 - p_1) \cdot (k_2 - p_1)) \left[\left(\left(\frac{p_1 \mp m_t n}{2} \right) \cdot q_2 \right) (p_2 \cdot q_1) - \left(\left(\frac{p_1 \mp m_t n}{2} \right) \cdot q_1 \right) (p_2 \cdot q_2) \right] \\
& \left. \pm \left(\frac{p_1 \mp m_t n}{2} \cdot p_2 \right) [((k_1 - p_1) \cdot q_2) ((k_2 - p_1) \cdot q_1) - ((k_1 - p_1) \cdot q_1) ((k_2 - p_1) \cdot q_2)] \right\},
\end{aligned}$$

and

$$\begin{aligned}
A_{m_t}^{(\pm)} = & \frac{|g|^4 |K_{ud}|^2}{(k_2^2 - M_W^2)^2} \frac{|g_{\pm}|^2}{2} \{ (m_t n \cdot p_2) [(p_1 \cdot q_2) ((k_2 - p_1) \cdot q_1) - ((k_2 - p_1) \cdot q_2) (p_1 \cdot q_1)] \\
& - (m_t n \cdot q_2) [(p_1 \cdot p_2) ((k_2 - p_1) \cdot q_1) - ((k_2 - p_1) \cdot p_2) (p_1 \cdot q_1)] \\
& + (m_t n \cdot q_1) [(p_1 \cdot p_2) ((k_2 - p_1) \cdot q_2) - ((k_2 - p_1) \cdot p_2) (p_1 \cdot q_2)] \\
& + m_t^2 [(q_2 \cdot p_2) (q_1 \cdot (k_2 - p_1)) + (q_1 \cdot p_2) (q_2 \cdot (k_2 - p_1)) - (q_1 \cdot q_2) (p_2 \cdot (k_2 - p_1))] \\
& \pm m_t (n \cdot (k_2 - p_1)) [(q_2 \cdot p_2) (q_1 \cdot p_1) + (q_1 \cdot p_2) (q_2 \cdot p_1) - (q_1 \cdot q_2) (p_2 \cdot p_1)] \\
& \mp m_t (p_1 \cdot (k_2 - p_1)) [(q_2 \cdot p_2) (q_1 \cdot n) + (q_1 \cdot p_2) (q_2 \cdot n) - (q_1 \cdot q_2) (p_2 \cdot n)] \},
\end{aligned}$$

and

$$\begin{aligned}
A_{m_b}^{(\pm)} = & \frac{m_b |g|^4 |K_{ud}|^2}{(k_2^2 - M_W^2)^2} \frac{g_{\pm}^* g_{\mp}}{2} \{ 2 (p_1 \cdot p_2) [(n \cdot q_2) ((k_1 - p_1) \cdot q_1) - (n \cdot q_1) ((k_1 - p_1) \cdot q_2)] \\
& - 2 (n \cdot p_2) [(p_1 \cdot q_2) ((k_1 - p_1) \cdot q_1) - (p_1 \cdot q_1) ((k_1 - p_1) \cdot q_2)] \\
& \pm i \varepsilon^{\mu\nu\alpha\beta} q_{2\alpha} q_{1\beta} (n_{\mu} p_{1\nu} (k_1 - p_1) \cdot p_2 + p_{2\mu} n_{\nu} (k_1 - p_1) \cdot p_1 + p_{1\mu} p_{2\nu} (k_1 - p_1) \cdot n) \\
& \mp i \varepsilon^{\mu\nu\alpha\beta} q_{2\alpha} q_{1\beta} (k_1 - p_1)_{\mu} [n_{\nu} (p_1 \cdot (k_2 - p_1)) + (k_2 - p_1)_{\nu} (p_1 \cdot n)] \\
& + (n \cdot (k_1 - p_1)) [(p_1 \cdot q_2) ((k_2 - p_1) \cdot q_1) - ((k_2 - p_1) \cdot q_2) (p_1 \cdot q_1)] \\
& - (n \cdot q_2) [(p_1 \cdot (k_1 - p_1)) ((k_2 - p_1) \cdot q_1) - ((k_2 - p_1) \cdot (k_1 - p_1)) (p_1 \cdot q_1)] \\
& + (n \cdot q_1) [(p_1 \cdot (k_1 - p_1)) ((k_2 - p_1) \cdot q_2) - ((k_2 - p_1) \cdot (k_1 - p_1)) (p_1 \cdot q_2)] \\
& + 2 m_t [(q_2 \cdot (k_1 - p_1)) (q_1 \cdot p_2) + (q_1 \cdot (k_1 - p_1)) (q_2 \cdot p_2) - (q_1 \cdot k_1) (q_2 \cdot k_1)] \\
& + m_t (q_1 \cdot q_2) [(p_2 \cdot p_1) + ((k_1 - p_1) \cdot (k_1 - p_2))] \}
\end{aligned}$$

$$\begin{aligned}
& +m_b^2 \frac{|g_{\pm}|^2}{2} \frac{|g|^4 |K_{ud}|^2 |K_{tb}|^2}{(k_2^2 - M_W^2)^2} \{ -m_t [(n \cdot q_2)(p_1 \cdot q_1) - (n \cdot q_1)(p_1 \cdot q_2)] \\
& +m_t^2 (q_1 \cdot q_2) - 2 \left[(q_2 \cdot (k_1 - p_1)) \left(q_1 \cdot \frac{p_1 \mp m_t n}{2} \right) \right. \\
& \left. + (q_1 \cdot (k_1 - p_1)) \left(q_2 \cdot \frac{p_1 \mp m_t n}{2} \right) - (q_1 \cdot q_2) \left((k_1 - p_1) \cdot \frac{p_1 \mp m_t n}{2} \right) \right] \},
\end{aligned}$$

Finally, it can be shown that we can obtain the other matrix elements from the above expressions performing the following changes

$$\begin{aligned}
|M_-^u|^2 &\longleftrightarrow |M_+^{\bar{u}}|^2 &\Leftrightarrow & n \longleftrightarrow -n, \\
|M_-^u|^2 &\longleftrightarrow |M_+^d|^2 &\Leftrightarrow & g_L \leftrightarrow g_R^*, \\
|M_-^u|^2 &\longleftrightarrow |M_-^{\bar{d}}|^2 &\Leftrightarrow & q_1 \leftrightarrow q_2,
\end{aligned} \tag{27}$$

it is useful to note also that all matrix elements are symmetric under the change

$$(n, g_L, q_1) \leftrightarrow (-n, g_R^*, q_2), \tag{28}$$

References

- [1] A.N. Okpara, hep-ph/0105151 and proceedings for the 36th Rencontres de Moriond, QCD and High Energy Hadronic Interactions, Les Arcs, France, March 17 - 24, (2001)
- [2] M.S. Chanowitz, Phys.Rev. D59 073005 (1999) and hep-ph/0104024
- [3] T.Appelquist and C.Bernard, Phys. Rev. D22 (1980) 200; A.Longhitano, Phys. Rev. D22 (1980) 1166; A. Longhitano, Nucl. Phys. B188 (1981) 118; R.Renken and M.Peskin, Nucl. Phys. B211 (1983) 93; A.Dobado, D.Espriu and M.J.Herrero, Phys. Lett. B255 (1991) 405.
- [4] T.Appelquist, M.Bowick, E.Cohler and A.Hauser, Phys. Rev. D31 (1985) 1676.
- [5] C.P.Burgess, S.Godfrey, H.Konig, D.London and I.Maksymyk, Phys. Rev. D 49 (1994) 6115; E.Malkawi and C.P.Yuan, Phys. Rev. D50 (1994) 4462, Phys. Rev. D52 (1995) 472.
- [6] See e.g. S.Catani, M.Mangano, P.Nason and L.Trentadue, Phys. Lett. B 378 (1996) 329.
- [7] T.M.P. Tait, Ph.D. Thesis, Michigan State University, 1999, hep-ph/9907462.
- [8] S.Dawson, Nucl. Phys. B249 (1985) 42; S.Willenbrock and D.Dicus, Phys. Rev. D34 (1986) 155; C.P.Yuan, Phys. Rev. D41 (1990) 42; R.K.Ellis and S.Parke, Phys. Rev. D46 (1992) 3785; G.Bordes and B. van Eijk, Z. Phys. C 57 (1993) 81, Nucl. Phys. B435

- (1995) 23; D.O.Carlson, Ph.D. Thesis, Michigan State University, 1995, hep-ph/9508278; T.Stelzer, Z.Sullivan and S.Willenbrock, Phys. Rev. D56 (1997) 5919.
- [9] T.Stelzer, Z.Sullivan and S.Willenbrock, Phys. Rev. D56 (1997) 5919 and Phys. Rev. D58 (1998) 094021
- [10] G.Mahlon and S.Parke, Phys.Rev.D55 (1997) 7249, Phys.Rev.D56 (1997) 5919, and Phys.Lett.B476 (2000) 323
- [11] F.Larios and C.P.Yuan, Phys. Rev. D55 (1997) 7218.
- [12] E.Bagan, D.Espriu, J.Manzano, Phys. Rev. D60, (1999) 114035.
- [13] D.Espriu, J.Manzano, Phys.Rev.D63, (2001) 073008.
- [14] C.Caso et al (The Particle Data Group), European Phys. J. C3 (1998) 1.
- [15] D.Amidei and C.Brock, *Report of the the TeV2000 study group on future electroweak physics at the Tevatron*, FERMILAB-PUB-96-082, 1996.
- [16] T.Swarnicki (for the CLEO collaboration), *Proceedings of the 1998 International Conference on HEP*, vol. 2, 1057.
- [17] F.Larios, M.A.Perez and C.P.Yuan, hep-ph/9903394; F.Larios, E.Malkawi, C.P.Yuan, Acta Phys. Polon. B27 (1996) 3741.
- [18] G.D'Ambrosio and D.Espriu, in preparation.
- [19] CTEQ4: H.-L. Lai et al., Phys. Rev. D55 (1997) 1280, <http://cteq.org>.
- [20] S.Parke, *Proceedings of the International Symposium on Large QCD Corrections and New Physics*, Hiroshima, 1997, Fermilab-Conf-97-431-T, hep-ph/9712512.
- [21] M. Fischer, S. Groote, J.G. Körner and M.C. Mauser, hep-ph/0101322
- [22] G.P.Lepage, Journal of Computational Physics 27 (1978) 192.
- [23] M. Jezabek and J. H. Kühn, Phys. Lett. B329, 317 (1994).
- [24] D.Espriu and J.Manzano, in *Proceeding of the 29 International Meeting on Fundamental Physics*, Sitges 2001, A.Dobado and V.Fonseca, eds.
- [25] S.Dawson, Nucl. Phys. B 249 (1985) 42.

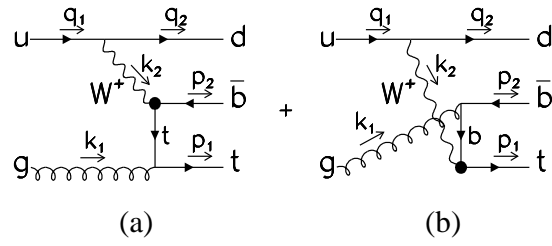


Figure 1: Feynman diagrams contributing single top production subprocess. In this case we have a d as spectator quark

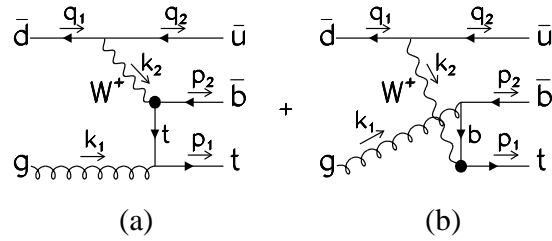


Figure 2: Feynman diagrams contributing single top production subprocess. In this case we have a \bar{u} as spectator quark

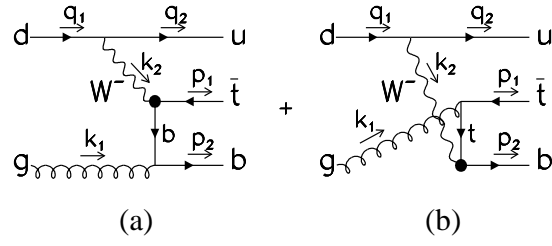


Figure 3: Feynman diagrams contributing single anti-top production subprocess. In this case we have a u as spectator quark

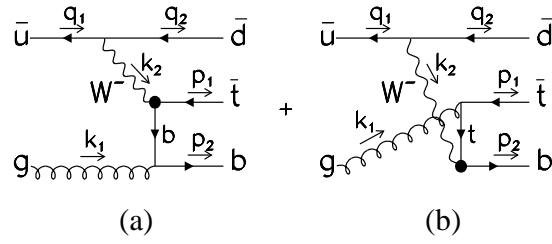


Figure 4: Feynman diagrams contributing single anti-top production subprocess. In this case we have a \bar{d} as spectator quark

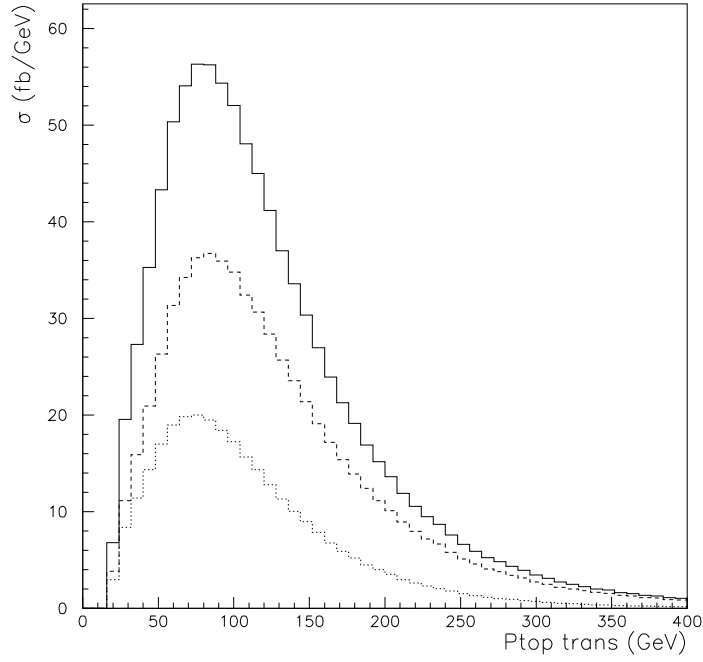


Figure 5: Top transversal momentum distribution corresponding to polarized single top production at the LHC in the LAB system. The solid line corresponds to unpolarized top production and the dashed (dotted) line corresponds to tops of negative (positive) helicity. The subprocesses contributing to these histograms have been calculated at tree level in the electroweak theory. The cuts are described in the text. The degree of polarization in this spin basis and reference frame is only 69% . The QCD scale is taken to be $\mu^2 = \hat{s} = (q_1 + q_2)^2$.

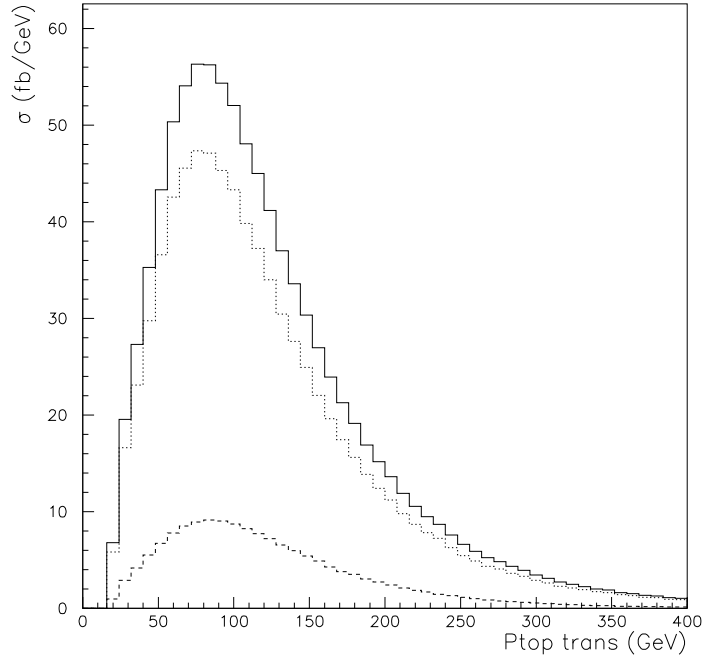


Figure 6: Top transversal momentum distribution corresponding to polarized single top production at the LHC. The solid line corresponds to unpolarized top production and the dashed (dotted) line corresponds to tops polarized in the spectator jet negative (positive) direction in the top rest frame. The subprocesses contributing to these histograms have been calculated at tree level in the electroweak theory. With our set of cuts, the polarization is 84 %. The QCD scale is $\mu^2 = \hat{s} = (q_1 + q_2)^2$

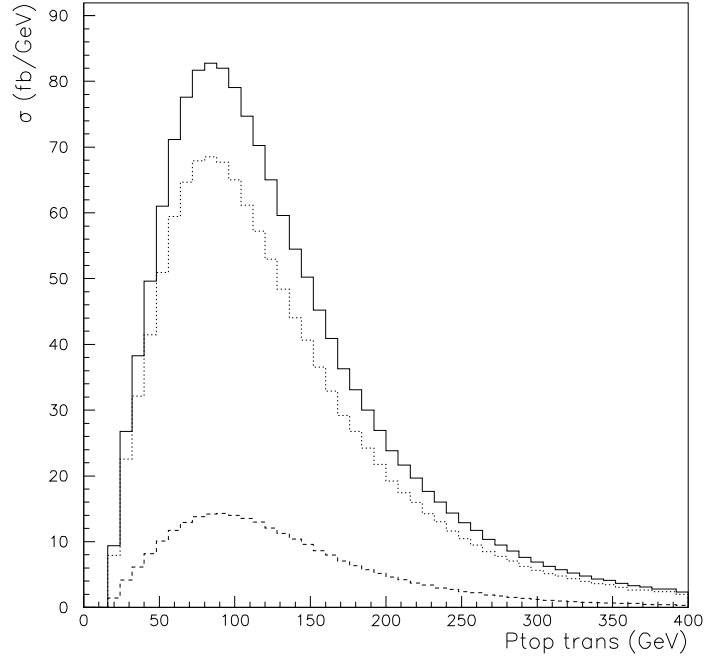


Figure 7: Here we plot the same histograms that in Fig.6. However here we have set the QCD scale $\mu = p_{cut}^{T(bot)} = 30$ GeV. For the gluon PDF we have also used this scale, but for the light quarks PDF's we have taken $\mu^2 = -k_2^2$ (the virtuality of the W). This is the set of scales taken by Stelzer et al in [9].

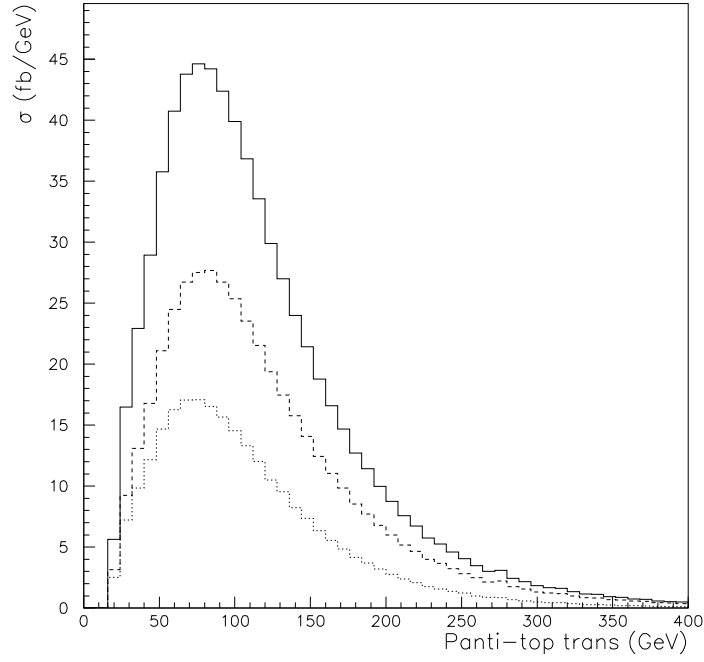


Figure 8: Anti-top transversal momentum distribution corresponding to polarized single anti-top production at the LHC. The solid line corresponds to unpolarized anti-top production and the dashed (dotted) line corresponds to negative (positive) helicity anti-top production. Same conventions and scale as in the previous figures.

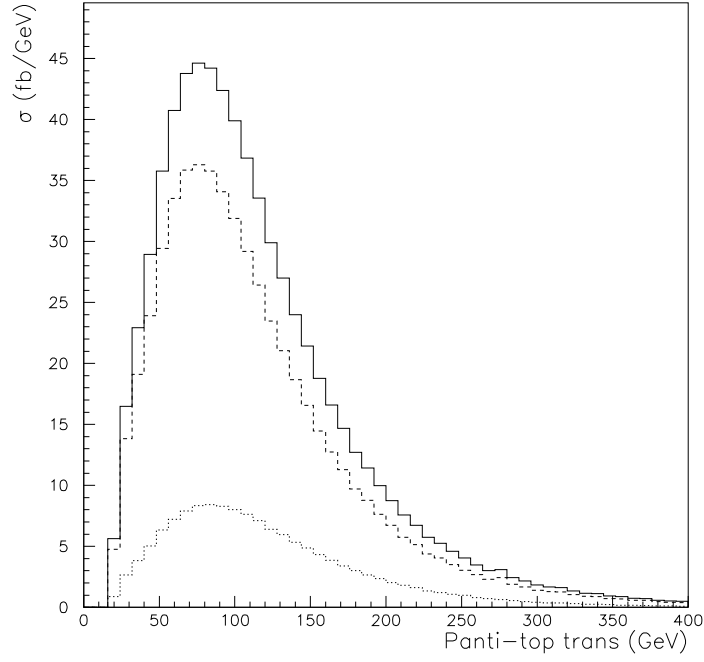


Figure 9: Anti-top transversal momentum distribution corresponding to polarized single anti-top production at the LHC. The solid line corresponds to unpolarized anti-top production and the dashed (dotted) line corresponds to anti-tops polarized in the spectator jet negative (positive) direction in the top rest frame. The subprocesses contributing to these histograms have been calculated at tree level in the electroweak theory, using the same cuts and conventions as in the previous figures.

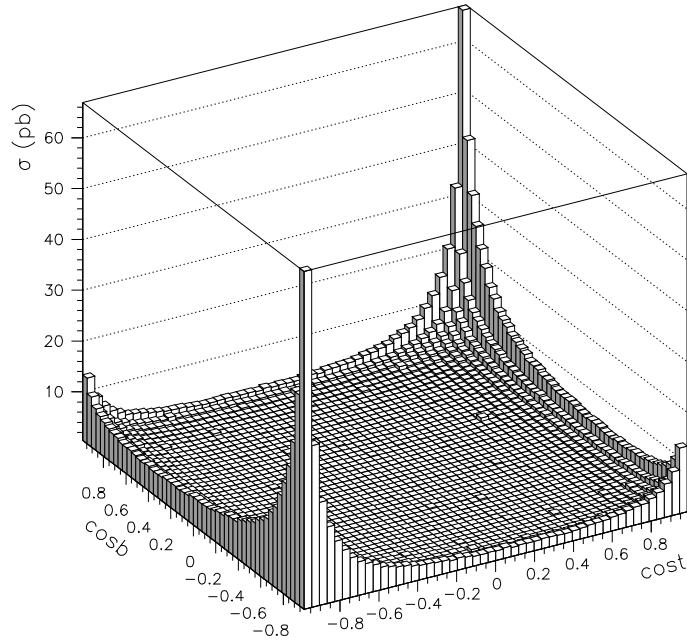


Figure 10: Distribution of the cosines of the polar angles of the top and anti-bottom with respect to the beam line. The plot corresponds to unpolarized single top production at the LHC. The calculation was performed at the tree level in Standard Model with $\mu^2 = \hat{s} = (q_1 + q_2)^2$.

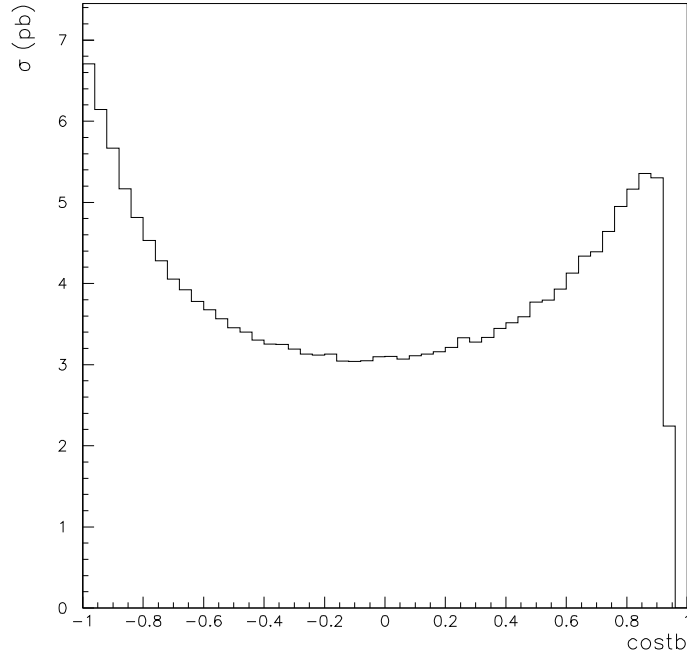


Figure 11: Distribution of the cosine of the angle between top and anti-bottom corresponding to unpolarized single top production at the LHC. The calculation was performed at the tree level in Standard Model with $\mu^2 = \hat{s} = (q_1 + q_2)^2$. The abrupt fall near 1 is due to the 20 degrees isolation cut.

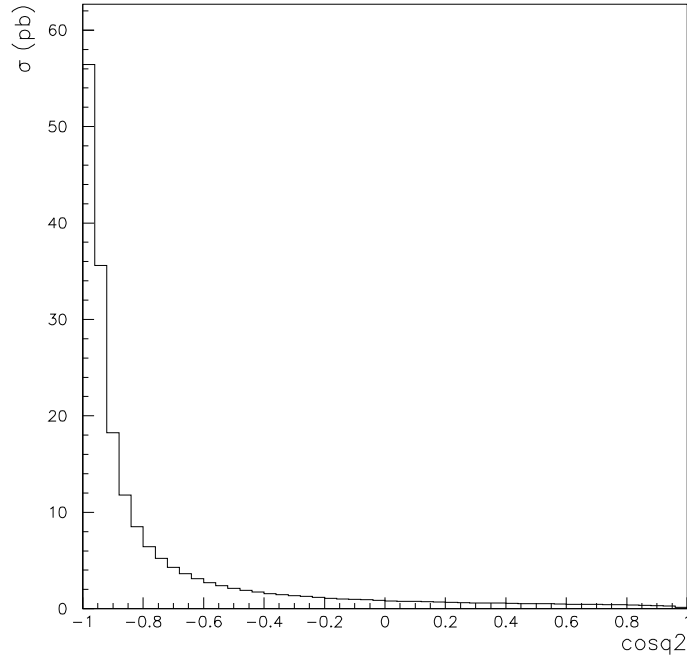


Figure 12: Distribution of the cosine of the angle between the spectator quark and the gluon corresponding to unpolarized single top production at the LHC. The momentum of the gluon is in the beam line direction but its sense is not observable so to obtain an observable distribution we have to symmetrize the above one. The calculation was performed at the tree level in Standard Model with $\mu^2 = \hat{s} = (q_1 + q_2)^2$.

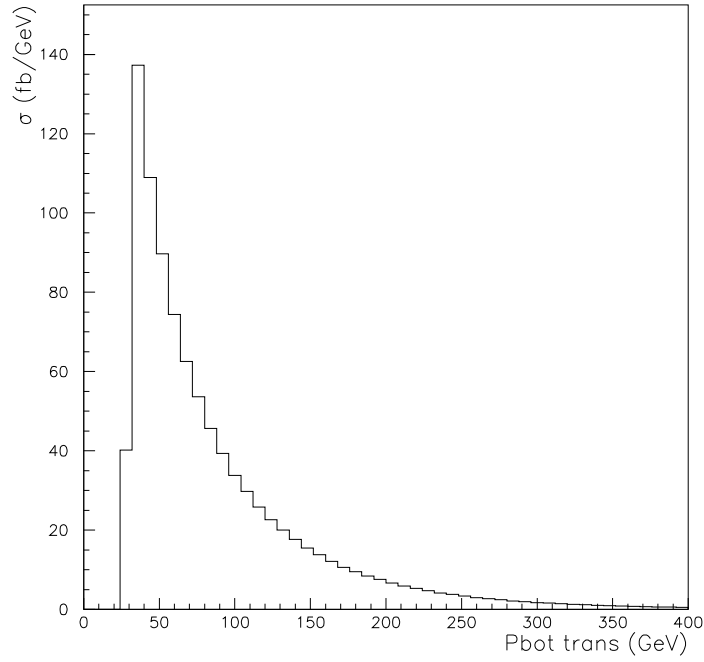


Figure 13: Anti-bottom transversal momentum distribution corresponding to unpolarized single top production at the LHC. The calculation was performed at the tree level in the Standard Model. Note the 30 GeV. cut implemented to avoid large logs due to the massless singularity in the total cross section. In this plot $\mu^2 = \hat{s} = (q_1 + q_2)^2$ too.

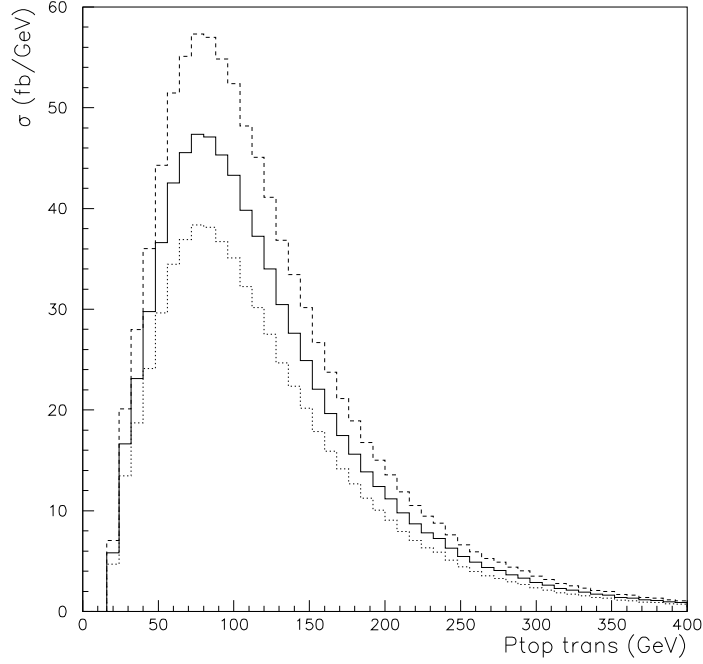


Figure 14: Top transversal momentum distribution corresponding to polarized single top production at the LHC. All plots correspond to tops polarized in the spectator jet *positive* direction in the *top rest frame*. The subprocesses contributing to the solid line histogram have been calculated at tree level in the SM ($g_L = 1, g_R = 0$). The dashed (dotted) line histogram have been calculated at tree level with $g_L = 1.1$, and $g_R = 0$ ($g_L = 0.9$, and $g_R = 0$). Note the roughly 20 percent variation in this cross section due to the variation of the left coupling around its SM tree level value

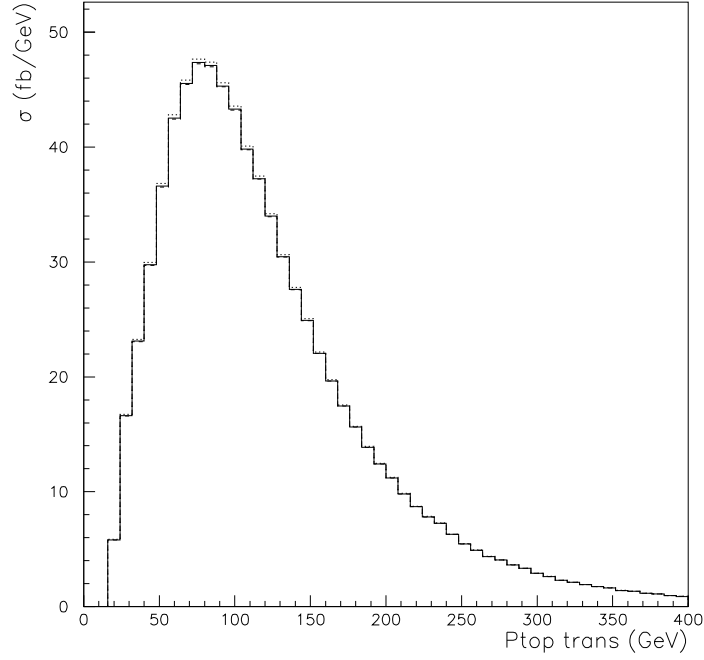


Figure 15: Top transversal momentum distribution corresponding to polarized single top production at the LHC. All plots correspond to tops polarized in the spectator jet *positive* direction in the *top rest frame*. The subprocesses contributing to the solid line histogram have been calculated at tree level in the SM ($g_L = 1$, $g_R = 0$). The dashed (dotted) line histogram have been calculated at tree level with $g_L = 1$, and $g_R = 0.1$ ($g_L = 1$, and $g_R = -0.1$). Note the variation in this cross section due to the variation of the right coupling around its SM tree level value is practically inappreciable.

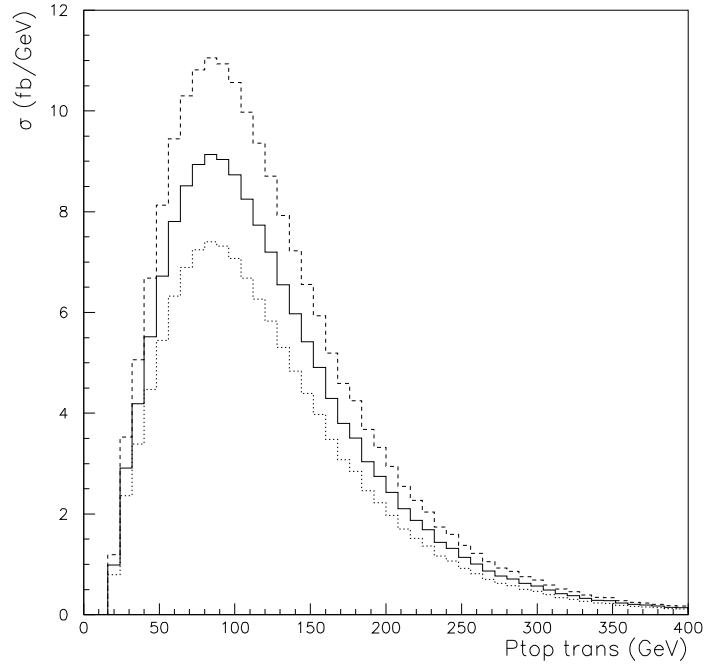


Figure 16: Top transversal momentum distribution corresponding to polarized single top production at the LHC. All plots correspond to tops polarized in the spectator jet *negative* direction in the *top rest frame*. The subprocesses contributing to the solid line histogram have been calculated at tree level in the SM ($g_L = 1, g_R = 0$). The dashed (dotted) line histogram have been calculated at tree level with $g_L = 1.1$, and $g_R = 0$ ($g_L = 0.9$, and $g_R = 0$).

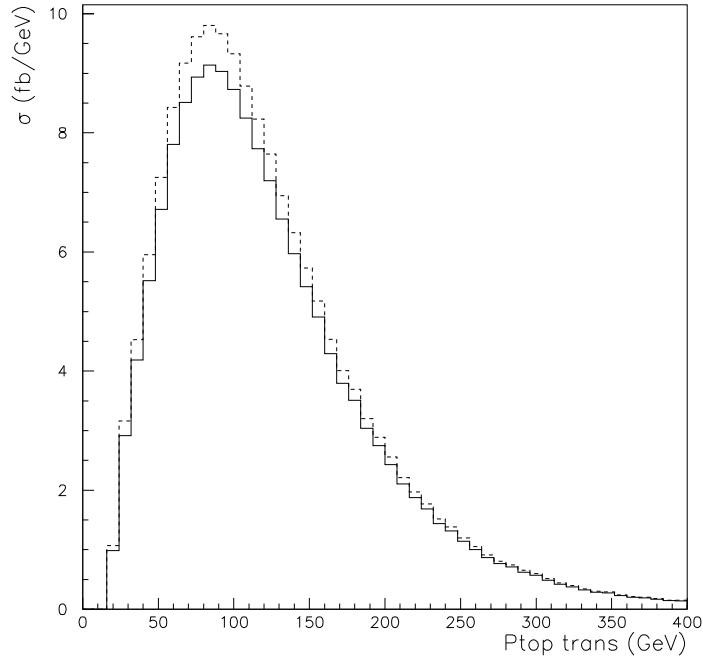


Figure 17: Top transversal momentum distribution corresponding to polarized single top production at the LHC. All plots correspond to tops polarized in the spectator jet *negative* direction in the *top rest frame*. The subprocesses contributing to the solid line histogram have been calculated at tree level in the SM ($g_L = 1$, $g_R = 0$). The dashed line histogram have been calculated at tree level with $g_L = 1$, and $g_R = -0.1$. The histogram corresponding to the couplings $g_L = 1$, and $g_R = 0.1$ has been omitted for the sake of clarity and it is located roughly in between the ones showed in the picture. Note that the sensitivity of this cross section to variations of the right coupling around its SM tree level value is comparable to the sensitivity to variations of the left coupling around its SM tree level value (see figure 16).